A high-throughput screening platform to identify nanocarriers for efficient delivery of RNA-based therapies

Vitor Francisco[1,2], Catarina Rebelo[1,2], Artur Filipe Rodrigues[1], Josephine Blersch[1], Hugo Fernandes[1,2], Lino Ferreira[1,2*]*

[1]Center for Neuroscience and Cell Biology, University of Coimbra, Coimbra, Portugal
[2]Faculty of Medicine, University of Coimbra, 3000-548, Coimbra, Portugal

Abstract

RNA-based therapies are highly selective and powerful regulators of biological functions. Non-viral vectors such as nanoparticles (NPs) are very promising formulations for the delivery of RNA-based therapies but their cell targeting, cell internalization and endolysomal escape capacity is rather limited. Here, we present a methodology that combines high-throughput synthesis of light-triggerable NPs and a high-content imaging screening to identify NPs capable of efficiently delivering different type of RNAs. The NPs were generated using polymers synthesized by Michael type addition reactions and they were designed to: (i) efficiently complex coding (mRNAs) and non-coding (miRNAs and/or lncRNAs) RNA molecules, (ii) allow rapid cell uptake and cytoplasmic release of RNA molecules and (iii) target different cell types based on their composition. Furthermore, light-responsive domains were attached to the polymers by distinctive methods to provide diverse disassembly strategies. The most efficient formulations were identified using cell-based assays and high-content imaging analysis. This strategy allows precise delivery of RNA-based therapies and provides an effective design approach to address critical issues in non-viral gene delivery.

Keywords (maximum 6)

RNA-based therapies, Nanoparticle library, Controlled release, High-throughput screening, High-content image analysis

1. Introduction

RNA-based therapeutics are one of the most attractive classes of drugs for treating a variety of diseases. Recently, there has been significant advances in the field of RNA-based therapeutics exploiting exogenous RNAs, including non-coding RNA such as small interfering RNA (siRNA) and microRNA (miRNA), as well as *in vitro* transcribed (IVT) messenger RNA (mRNA) [1-3]. RNA-based therapeutics offer numerous advantages compared to the conventional small molecule-based therapies, such as the precise control over the production of proteins of interest with minimal off-target effects [4]. However, there are several obstacles to overcome in the application of RNA-based therapeutics in the clinic including (i) poor stability and biological half-life of RNAs when administered in the bloodstream, (ii) limited efficacy in terms of organ/tissue targeting and (iii) limited endolysosomal escape capacity within the target cell [5].

Polymeric materials are attractive candidate vehicles for RNA-based therapeutics due to their low immunogenicity, low cost, easy of production and chemical versatility ultimately enabling high-throughput strategies to study structure-activity relationships in specific cell populations [6, 7]. Cationic polymers, such as poly(amido amine)s (PAAs), have been used for gene delivery both *in vitro* and *in vivo*, but with limited efficiency and targeting [8]. Therefore, polymer engineering strategies have focused on chemically modifying polymers to increase their charge and/or hydrophobicity, in order to improve the complexation efficiency of RNA molecules [9]. For example, PAAs have been modified with ethylenediamine or triethylenetetramine to increase the polymer´s positive charge and thus improving siRNA binding [10]. Other formulations have been developed to lower the excessive binding affinity of the nanocarrier towards RNA molecules [11]. Yet, further advances are necessary for the development of polymeric materials with high delivery efficiency and targeting potential.

Light-sensitive materials have gained attention in recent years as potential vehicles for RNA-based therapeutics because they are able to release the cargo with spatiotemporal control

thus increasing the transfection efficiency and targeting in specific cells [12-14]. Studies have shown that the efficiency of cytosolic delivery of RNA-based therapeutics increased a few minutes after being internalized by the cell [15]. Recently, we reported the synthesis of two light-sensitive libraries of 110 and 160 structurally unique PAAs using high-throughput combinatorial chemistry to form NPs vectors for RNA-based therapeutics [16, 17]. Several criteria were met when designing the gene delivery NPs that can eventually be produced on an industrial scale and used in a clinical setting. Specifically, the synthesis pathway had the following features: (i) inexpensive synthesis, (ii) ease of fabrication, (iii) facile purification and (iv) cheap storage whilst maintaining stability [18]. Our results showed that the top formulations of both libraries were more efficient than commercial reagents, such as lipofectamine, for the delivery of RNA-based therapeutics.

Here, we describe a methodology to identify nanocarriers for the efficient delivery of different type of RNAs that combines high-throughput synthesis of light-triggerable NPs and high-content imaging screening. The methodology includes the synthesis of the polymers, the preparation of the NPs, a procedure for the complexation of different RNA molecules, the physico-chemical characterization of the NPs and finally the evaluation of the cargo activity delivered by the NP in cellular models. We provide information regarding the influence of the monomer selection, light responsiveness moieties, cargo loading and cellular uptake on the transfection efficiency. The methodology described here may inspire researchers for the development of their own libraries of drug delivery systems or the use of this set up to screen commercial available transfection agents.

2. Materials and methods

2.1 Polymer synthesis for method 1

Bisacrylamide monomers (labelled A-E, 2200 μL) and diamine (numbered 1-22, 600 μL) were prepared in anhydrous DMSO at a final concentration of 1.6 M. Subsequently, each

bisacrylamine monomer was mixed with each diamine monomer (1:1; 100 μL of each) into a 96-deepwell plate, the plate was sealed with aluminum foil, incubated on an orbital shaker for 5 days at 60 °C, 250 rpm. Following, 20 μL of the respective diamine was added to each well and incubated for further 2 h to obtain amine endcapped polymers. The obtained solution was maintained on the orbital shaker, the temperature was adjusted to 25 °C and 180 μL of anhydrous DMSO with triethylamine (10% molar ratio to NVOC (4,5-dimethoxy-2-nitrobenzyl chloroformate) added. Finally, NVOC (molar ratio of 1:4.5 (NVOC:diamine)), in solid form, was added to each well and the plate was incubated on an orbital shaker for 24 h at room temperature (RT).

2.2 Polymer synthesis for method 2

P1 was prepared by adding triethylamine (10.5 mL, Sigma-Aldrich) to (2-nitro-1,3-phenylene)dimethanol (5.5 g, 30 mmol, ARCH Bioscience) in anhydrous dichloromethane (38 mL, Fisher Chemical), under argon atmosphere at room temperature. After stirring the mixture for 1 h, the temperature was adjusted to 0 °C, acryloyl chloride (9.8 mL, 120 mmol, Merck) was added in a dropwise manner and the mixture was stirred for 18 h at room temperature. Subsequently, the mixture was filtered to remove the formed solid, the filtrate was dried under vacuum, the resulting residue resuspended in ethyl acetate, washed with saturated sodium chloride and dried overnight with sodium sulfate. Finally, P1 was obtained as a white crystal by purification of the crude product by silica gel chromatography using hexane:ethyl acetate as eluent (1:1, v/v).

Bisacrylamide monomers (labelled A-E, 1600 μL), P1 (8000 μL) and amine (labelled 1-32, 600 μL) were prepared in anhydrous DMSO at a final concentration of 1.6 M. Subsequently, each bisacrylamide monomer was mixed with P1 (1:1, 50 μL), 100 μL of each amine was added into a 96-deepwell plate, the plate was sealed with aluminum foil, incubated on an orbital shaker for 5 days at 60 °C, 250 rpm. Next, 20 μL of the respective diamine was added to each well and incubated for further 2 h to obtain amine end-capped polymers.

2.3 Nanoparticle synthesis

For the synthesis of the NP, 15 μL of each polymer was added to 960 μL of water in a 96-deepwell plate and subsequently 25 μL of zinc sulfate (1.0 M) was added and the mixture was incubated on an orbital shaker for 24 h at RT, 250 rpm. Upon incubation, the formulation was transferred to a 2.0 mL tube, centrifuged for 8 min at 8000g, 4 ºC and finally resuspended in 1 mL of water (molecular biology grade).

2.4 Nanoparticle characterization

NPs were lyophilized and 200 μL of each formulation was used to determine NP concentration and formation efficiency. To determine NP size, each formulation (50 μg/mL in 1.5 mL in water) was analyzed by dynamic light scattering (DLS). Moreover, to determine NP disassemble efficiency upon exposure to UV light, each NP formulation was irradiated with UV light (10 min, 365 nm, 100 mW/cm^2) and the NP count was calculated. NP count decrease was expressed as a percentage of decrease respective to the initial average count. To determine the zeta potential, KCl (1 mM) was added to each formulation (50 μg/mL in 1.5 mL) and analyzed by DLS.

2.5 Complexation of siRNA with NPs

To study the complexation of siRNAs with NPs, 100 μL of each NP (400 μg/mL) was added to 100 μL of siRNA (8 μg/mL; 4 μg/mL siRNA + 4 μg/mL siRNA-Cy5) in a 2 mL tube and incubated for 2 h at RT in an orbital shaker, 250 rpm. Subsequently, the solution was centrifuged at 8000g for 8 min at 4 ºC, the supernatant was collected and the fluorescence measured in a plate reader to determine the amount of siRNA on the NP surface. Complexation efficacy was determined indirectly from Cy5 tagged-siRNA, whereas the concentration of siRNA was determined relative to a standard curve, $y = 5383x$ ($R^2 = 0.9988$).

2.6 High-throughput screening of RNA delivery.

HeLa-GFP cells (CellBiolabs Inc.) and Cre reporter fibroblasts (kindly donated by Dr. Carol Stocking, University of Hamburg, Germany [19]) were cultured in DMEM containing FBS (10%, v/v) and PenStrep (0.5%, v/v, 50 µg/mL). Prior to transfection, cells were seeded into 96 well plates (Costar) at a density of 4000 cells and 3000 cells per well, respectively. After 24 h, cells were transfected with the tested formulations and with the commercial agents Lipofectamine RNAiMAX® and Lipofectamine2000® in DMEM. Transfections were performed in three independent experiments (n=3).

For siRNA transfections, a 10 min transfection protocol was optimized. In brief, NPs (20 µg/mL) previously complexed with the siRNA were added to the cells in DMEM (without FBS and PenStrep) using a multichannel pipette. After 10 min of transfection, the medium was replaced by DMEM containing 5% FBS (v/v, to slow down cell proliferation), PenStrep and blasticidin (10 µg/ml). To compare the bioactivity of released siRNA with and without application of the stimulus, NPs were activated for 10 min with 365 nm light, applied from the top, using a transilluminator UVP BioSpectrum 500 at 15 cm distance. As a control we used the same NP formulations but without light activation. After 48 h, nuclear staining was performed and analyzed by high-content imaging with an automated fluorescence microscope (In Cell Analyzer 2200, GE Healthcare; see details below).

For the hard to transfect long coding mRNA, transfection was extended to 4 h. In this case, immediately before transfection, polymers (5 µg/well) and Cre mRNA (50 ng/well) were complexed in molecular grade nuclease free sterile water. After homogenization of the mixture using a multichannel pipette, the polyplex suspension was maintained for 10 min at room temperature for complexation. Subsequently, suspensions were diluted in DMEM (without FBS and PenStrep) and used to transfect the cells. After 4 h of incubation, the media (and remaining particles) was removed by pipetting and the media was replaced with fresh warmed complete DMEM containing FBS and PenStrep. After 48 h, nuclear staining was performed and analyzed by high-content imaging with an automated fluorescence microscope (In Cell Analyzer 2200, GE Healthcare; see details below).

2.7 High-content imaging analyses.

After 48 h of culture, cell nuclei were stained with Hoechst H33342 (0.25 µg/mL) and propidium iodide (PI; 0.25 µg/mL) and automated imaging was performed using the IN Cell Analyzer 2200 Cell Imaging System (GE Healthcare). At least four random fields per well were taken with a 20x objective and images were analyzed in the IN Cell Developer and IN Cell Analyzer software.

Program A: the IN Cell Developer software was used to evaluate GFP knockdown. A nuclear segmentation mask was defined based on the nuclear staining (minimum target area 408 pixel and sensitivity 45 with clump breaking postprocessing) and used to quantify the number of cells per area. Cells were considered dead if the nuclear staining overlapped with PI (10% overlap between the nuclear mask and a PI intensity-based segmentation mask). Cell viability was calculated from the total number of cells (based on nuclear count) after subtraction of dead cells. GFP knockdown was assessed from the mean green fluorescence intensity in the cytoplasm of live cells. For this evaluation, a cell segmentation was defined by dilation and clump breaking post-processing of the nuclear segmentation to cover as much of the cytoplasmic region as possible (collar segmentation). The cytoplasm was defined by subtraction of the nuclear mask on the cell mask. GFP knockdown was expressed as the percentage of fluorescence on non-treated HeLa-GFP cells (after subtracting fluorescence background of HeLa cells). Internalization of NPs was quantified based on the fluorescence signal of NP@siRNA-Cy5 in cells.

Program B: Cre-mRNA recombination was followed based on the green fluorescence intensity in the cytoplasm of live cells. For this purpose, we used the In Cell Analyzer software for a multi-target analysis assay. Hoechst was used to define a nuclear mask and quantify the number of cells. In brief, nuclear identification was performed using the software top-hat method (minimum area 80 μm^2 and sensitivity of 90). Cells with nuclear intensity (Nuc Intensity CV) above the defined threshold were identified as having nuclear condensation and were removed from the analysis (dead cells). Cell viability was calculated from the total number of

cells (based on nuclear count) after subtraction of dead cells. The nuclear mask was then dilated to cover as much of the cytoplasmic region as possible using the collar segmentation method (radius 3 µm). The cytoplasm mask was defined as the ring-like structure resulting from this segmentation. GFP expressing cells were quantified as the cells with a green intensity in the cytoplasm (Cell/Bckg Intensity in the green channel) above the negative control. Recombination efficiency was calculated as the percentage of viable cells positive for GFP expression.

2.8 Protein expression analysis. Cre reporter fibroblasts (10^5 cells/well) were seeded in 6-well plates and treated with Lipofectamine® 2000 complexed for 10 min with Cre mRNA, according to the manufacturer's instructions. For flow cytometry, cells were stained with PI (1 µg/mL) and dissociated using 0.05% (w/v) trypsin-EDTA in PBS 1x, followed by centrifugation at 300 g for 3 min. Cell suspensions in PBS 1x were obtained and analyzed using a BD Accuri C6 flow cytometer (BD Biosciences). Cell viability and GFP fluorescence were analyzed using FlowJo software (version X.0.7, FlowJo LLC).

For Western blot analysis, cells were lysed in RIPA buffer supplemented with a protease/phosphatase inhibitor cocktail (Cell Signaling Technology). Total protein content was quantified using a Pierce BCA Protein Assay kit (ThermoFisher Scientific). Cell samples (20 µg protein) were denatured in Laemmli buffer (Alfa Aesar) after heating for 5 min at 95°C, and loaded onto a 4% acrylamide stacking gel placed on top of a 10% running gel. Electrophoresis was performed at 80 V for 15 min, followed by 75 min at 140 V. Separated proteins were transferred to a PVDF membrane (BioRad) for 90 min on ice at 100 V. The blots were blocked with 5% (v/v) bovine serum albumin (BSA) in tris-buffered saline with Tween 20 (0.1%) (TBS-T, Tris) for 45 min, followed by overnight incubation with primary antibody in 1% BSA in TBS-T at 4 °C. Primary antibodies used in this study were: rabbit anti-Cre recombinase (Abcam, ab190177; 1:2000), rabbit anti-GFP (Abcam, ab6556; 1:2000), and rabbit anti-β-tubulin (Cell Signaling Technologies, #2128; 1:1000). Membranes were then washed with TBS-T and incubated with HRP-linked goat anti-rabbit IgG (Cell Signaling, #7074; 1:2000) in 1% BSA in

TBS-T for 1 h. After washing the membrane with TBS-T, membranes were incubated with Chemiluminescent Peroxidase Substrate (Sigma Aldrich) and visualized using a ChemiDoc-It scanner (VWR).

2.9 RT-qPCR analysis. Cells were lysed and total RNA was extracted using an ad hoc kit (RNeasy Mini Kit, QIAGEN), according to the manufacturer's instructions. Concentration and purity of extracted RNA were determined by measuring the optical density at 260, 280 and 230 nm, using a NanoDrop spectrophotometer (ThermoFisher Scientific). First-strand complementary DNA (cDNA) was generated from 1 µg RNA in a total volume of 20 µL using the cDNA Supermix (QuantaBio). Reverse transcription was performed using the CFX96 real-time PCR detection system (BioRad). Polymerase chain reaction was carried out using 1 µL cDNA, 200 nM of each primer and 5 µL NZYSpeedy qPCR Green master mix (NZYTech) in a 10 µL reaction. After a denaturing step at 95 ^{o}C for 10 min, amplification consisted of 40 cycles of denaturation at 95 ^{o}C for 10 s intercalated with annealing and elongation at 60 ^{o}C for 30 s. Finally, a melting curve analysis confirmed PCR product specificity and lack of signal in non-template controls. Relative gene expression was calculated using the Livak (ΔΔCt) method, assuming GAPDH as the housekeeping gene to normalize gene expression. The following PCR primer sequences were used in this study (presented in 5'-3' orientation): Cre-Fwd: ACGACCCCAACAACTACCTG; Cre-Rev: CACGACCCCAACAACTACCTG; GFP-Fwd: ACGACGGCAACTACAAGACC; GFP-Rev: TTGTACTCCAGCTTGTGCCC; GADPH-Fwd: ACCACAGTCCATGCCATCAC; GADPH-Rev: TCCACCACCCTGTTGCTGTA.

3. Results and discussion

3.1 Polymer reaction type and monomer selection. The synthesis of light-triggerable NP libraries for the delivery of RNA-based therapeutics should take advantage of simple synthetic schemes, avoiding long purification steps. We have used two principles for the preparation of those libraries (Fig. 1). For the first library, the polymers were synthesized and reacted with a

photocleavable molecule that was positioned as a pendant molecule, while for the second library, a photocleavable linker (PCL) was introduced onto the chain backbone. PAAs were synthesized by Michael-type addition of bisacrylamide monomers with amines (Fig. 1B). The rationale for employing the versatile Michael addition reaction as a strategy to synthesize the polymers was based with the large range of possibilities for the selection of monomers and functional precursors, mild reaction conditions as well as high conversions and favorable reaction rates [20]. Monomer selection was based on previously reported NP libraries for RNA delivery [21, 22]. It has been reported that NPs with piperazine (monomer E, 11, 31), pyrrolidine (monomer 29) or imidazole groups (monomer 30) in the structure of the polymer showed enhanced complexation, delivery and internalization [22, 23]. In addition, NPs composed of polymers containing two amines in close proximity (monomer 1, 2, 4, 5, 6, 7, 8, 16, 18) were able to successfully avoid trafficking to lysosomes [23, 24]. Moreover, polymers with disulfide linkages (monomer C) were stable under physiological conditions but underwent fast degradation in the reductive environment of the cytosol [25].

Distinctive photocleavable molecules were selected to design the light-responsive NPs. In the first library, the commercial photocleavable linker, 4,5-dimethoxy-2-nitrobenzyl chloroformate (NVOC) was attached to the PAAs by reaction with amines, while in the second library we prepared a symmetrical bifunctional photocleavable monomer suitable for the condensation reaction between the selected monomers. In order to achieve the highest NP disassembly upon light triggering, it was critical to optimize the ratio of the photocleavable group inserted into the polymer (Fig. 1B). Lower ratios of photocleavable groups in the polymer could lead to inefficient NP disassembly while higher ratios could result in poor NP stability or slower disassembly. In library 1, the best ratio was obtained with a 20% degree of substitution of NVOC while in library 2, the best NP disassembly after light triggering was obtained when 25% of the photocleavable group was inserted in the polymer backbone [16].

After the synthesis of the polymers, they were nanoprecipitated in water and their physico-chemical properties (size and zeta potential) and capacity to disassemble after exposure to UV/blue light (Fig. 2) were characterized. NP average size (310 ± 192 nm *versus* 405 ± 242 nm for method 1 and method 2, respectively) and zeta potential (13.8 ± 10.1 mV *versus* 12.7 ± 8.6 mV for method 1 and method 2, respectively) were similar (Fig. 3). However, light responsiveness was significant different for both libraries. In library 1, only 52.5% of the formulations had a NPs count decrease higher than 50% when irradiated with UV light while in library 2, the percentage of NPs with count decrease higher than 50% after irradiation was 82.7%. However, both polymeric libraries used photoisomerization of o-nitrobenzyl groups into o-nitrosobenzaldehyde species upon UV light, and the percentage of photolabile group in the polymer was similar (~20 and 25%). This result may be explained by the differences in polymer structure after UV irradiation, due to differences between placing the photo-breakable unit in the side-chain as pendant or in the polymer main-chain. In library 1, the incomplete cleavage of NVOC moiety after UV light irradiation led to intact polymer main-chain with certain hydrophobicity (from NVOC) that could prevent NP disassembly (Fig. 4A), while in polymers obtained by method 2, the polymer main-chain was transformed into smaller species and therefore increased the probability of NP disassembly. (Fig. 4B).

The NPs synthesized by both methods covered the main categories of photoresponsive polymers: one was for polymers in which the chromophores were attached as pendants to already synthesized polymers, while the other covered polymers whose chromophores species were incorporated into polymer main-chain. There are some advantages and disadvantages in each method to synthesize libraries of photoresponsive NPs. With method 1, one could modify natural polymers, such as chitosan, dextran, hyaluronic acid, or commercially available polymers, such as polyethylenimine (PEI) or polylysine, with NVOC, in order to increase the hydrophobicity of these water-soluble polymers and thus to form NPs. Although with method 2 it is possible to modify natural polymers to be photoresponsive, in particular those with low molecular weight, probably the low hydrophobicity of these synthesized polymers prevents the formation of NPs. On the other hand, with method 2, one

could rationally design and construct a large diversity of main-chain photodegradable polymers with diverse macromolecular structures and functions. As an example, this method can be easily used for the synthesis of photoresponsive libraries of poly(β-amino ester)s which, despite their biodegradability, usually suffer from slow degradation of polymer main-chain. When compared with method 1, polymers synthesized by method 2 produced nanomaterials that undergo more severe modification in their structure and morphology upon irradiation with light.

3.2 Complexation of RNA molecules. Strategies to package and deliver RNA molecules using NPs include physical entrapment within NP matrix, covalent bonding and electrostatic surface interaction. The packaging must be sufficient to protect the RNA from enzymatic degradation prior to cytosolic delivery, whilst still able to fully unpack or dissociate from the carrier before being functionally incorporated into the RISC complex. Binding of RNA molecules can be particularly challenging depending on their length. Shorter molecules, such as siRNA and miRNA, have lower binding points with the cationic polymers, when compared with longer mRNA. For other polymeric gene delivery systems, the relationship between molecular weight and gene delivery has been associated with variation in NP size, charge and transfection efficiency [26].

For small RNAs (miRNA and siRNA; ~20 kDa), we have explored the packaging at the surface of the NP by electrostatic interactions. This strategy was adopted because it allowed us to characterize the NP before RNA complexation giving us a better control over the final formulation as well as a better knowledge of structure-activity relationship. Moreover, this strategy allows the generation of formulations purer than the ones obtained from the complexation of the RNA with the polymer for the formation of the NP. We anticipated that NPs with higher zeta potential could have higher affinity for RNA molecules; however, our results showed that was not the case. When comparing NPs formed by methods 1 and 2 with each other, NPs obtained by method 1 perform slightly better in the complexation of siRNA,

although it was difficult to find a complexation efficiency trend. NPs formed by both methods showed NPs with zeta potential lower than + 10 mV which were able to complex almost 100 % of RNA molecules. These results suggest that siRNA complexation depends primarily on chemical composition of NPs and not NP charge density (Fig. 3B and 3D).

Although the complexation of small RNA (miRNA and siRNA) molecules at the surface of the NPs was relatively easy and efficient, the complexation of large RNA molecules (~1000 kDa), such as mRNA, was relatively difficult. The complexation behavior of mRNA with pre-formed NPs or as polyplexes (i.e., when the polymer was mixed with mRNA to form the NP) was investigated by agarose gel analyses. For these assays, we have used two polymers, i.e., P1E28 and P1C5, at various weight ratios (Fig. 5). Our results showed that polyplex NPs retarded migration of mRNA from w/w ratio 1:1 with P1E28 or P1C5 polymers, respectively, while with pre-formed NPs, retardation was only observed for ratio 1:100 or 1:5. These results showed the higher ability of the polymers to complex mRNA as polyplex than complexation of mRNA on the surface of already formed NPs.

3.3 Cell Model. Cell-based assays are required to identify NP formulations that combine high biological activity with reduced cytotoxicity. In addition, cell-based assays may give critical information about NP internalization and intracellular trafficking. Primary cells, cell lines or engineered cells may be used to this end. Primary cell culture is the option that more closely relates to the physiological context [27]. On the other hand, cancer cell lines present specific characteristics that hinder their use for *in vivo* applications in a full organism. Although cancer cell lines are normally easier to culture than primary cells, they differ genetically and phenotypically from their tissue of origin [28, 29]. Engineered cells may be useful to show knockdown or gene editing activities for a particular formulation. In our experiments, we have used engineered cancer cells (HeLa) or fibroblasts (SC-1), expressing GFP protein or integrating a LoxP construct in their genome, respectively, in order to study the effect of the selected RNA-based therapies. In these studies, we have used HTS to evaluate the delivery

of RNA therapeutics: small non-coding RNAs for the knockdown of protein expression or messenger RNA (mRNA) for the overexpression of proteins of interest. In the case of HeLa-GFP cells, we used GFP knockdown as a measure of RNA delivery and formulation efficiency. This method allowed us to follow up over-time RNA delivery without the need for endpoint assays. The delivery of a mRNA encoding the fluorescent GFP protein can be followed in any cell system without the need for an engineered cell. However, multiple molecules must be delivered to the same cell in order to achieve measurable protein translation through a strong fluorescent signal. Alternatively, several reporter systems have used other mRNA cargos to study the delivery of these molecules, namely *in vivo* [30-32]. Cre recombinase mRNA is an alternative to GFP mRNA that allows a permanent and strong modification in the cells' genome. Cre catalyzes a recombination process in between two specific sequences (loxP sites) [33]. This enzyme can be used for the excision of a stop codon and subsequent expression of a fluorescent reporter gene. For example, for the evaluation of Cre mRNA delivery, we used engineered fibroblast that have a LoxP-flanked GFP cassette and only upon recombination the expression of GFP is detected [19]. In this case, one single molecule of mRNA successfully delivered intracellularly should result into a strong fluorophore expression, allowing a clear identification of formulations that deliver mRNAs, even if at lower efficiencies, a critical requirement for difficult to transfect mRNA molecules. Overall, there are several cell-based systems that can be harnessed to address a similar biological question. The selected cell line will depend on the available tools, but it must represent an adequate model for the addressed question.

Concomitantly to the selection of the cell type, biological controls need to be considered in cell-based high-throughput assays. When screening a large number of candidates, it is important to normalize and validate your data based on the correct selection of positive and negative controls. Furthermore, it is important to compare the new formulations with well-established commercial agents such as Lipofectamine2000 [30] and Lipofectamine-RNAiMAX [31]. In our experiments, we have used both commercial agents as positive controls for transfection.

3.4 – High-content imaging. Fluorescence is one of the most used readouts for high-throughput analyses. In comparison with other readouts, such as luminescence, fluorescence allows simultaneous and multiple readouts based on the appropriate selection of fluorophores that can be used in parallel (without crossover of emission wavelengths). Moreover, fluorescence can be quantified in several manners and places within the cells such as intensity, cellular localization, lifetime and even resonance energy transfer in between adjacent fluorophores. While classic techniques to measure fluorescence are usually end-point data from plate-readers or labor-intensive microscopic analysis, the recent developments in automated microscopy and correspondent imaging analysis has allowed the scalability of image analysis and generation of cell-based high content screenings with fluorescence as a read-out. High-content imaging analysis is a powerful tool in cell-based high-throughput assays. For the identification of efficient transfection agents, this technique can address, in the same experiment, readouts of cellular viability (Hoechst and PI staining), internalization of fluorescent-labeled formulations and successful outputs of RNA delivery (fluorescent protein knock-in or knock-out). For example, we evaluated HeLa-GFP cell viability upon transfection with NPs and exposed with UV light. The high-content imaging analyses showed low (<5%) impact in cell viability after exposure to UV light or fragments from NPs upon disassembly (Fig. 6).

The physicochemical properties, such as composition of the formulations, size and surface charge, play a key role in the cellular uptake of NPs, and consequently on RNA delivery [34, 35]. To evaluate the role of NPs physicochemical properties on cellular uptake and GFP knockdown activity, libraries complexed with siRNA-Cy5 were added to HeLa-GFP cells. Our results showed that cellular uptake was not uniquely driven by the charge of the NP since some formulations with low zeta potential have high cellular internalization, such as E1, A1 or P1B11, while some NP formulations with high zeta potential have low cellular internalization, as A15 or P1D23 (Fig. 7). The results obtained with both libraries suggest that although surface charge is an important parameter determining cellular uptake efficiency, similarly to reports from others [36-38], factors such as compositional elements of the formulations,

protein corona formation, aggregation/agglomeration are also important for cellular uptake. In addition, the correlation plot between GFP knockdown and NP properties, such as responsiveness to the UV trigger, siRNA complexation and cellular uptake, showed limited prediction at finding the best formulations to transfect RNA molecules (Fig. 8). Indeed, the data obtained from the best 10 formulations of each library showed that none of the 3 parameters analyzed, i.e., NPs disassembly, siRNA complexation efficiency and cellular internalization, correlated with the formulation activity. It is possible that intracellular trafficking (not evaluated in the context of this work) plays a crucial role in this process and thus it should be carefully examined in the future studies.

3.5 – Benchmarking with conventional techniques. High-content imaging presents additional advantages in screening formulations compared to traditional techniques used to analyze gene expression (Fig. 9). Quantitative reverse transcription polymerase chain reaction (qRT-PCR) is the main technique used to quantify RNA, after reverse transcription to complementary DNA (Fig. 9B). This cDNA serves as a template for PCR in order to quantify the expression of target genes. Although it is highly specific and sensitive, RT-qPCR detects total extracted mRNA, irrespective of its functional delivery. Hence, this method does not distinguish delivered mRNA (capable of being translated into proteins) from mRNA retained in endosomes or interacting with cell membranes with no effective uptake [30].

Moreover, Western blot is the gold-standard to quantify protein expression, but it is time-consuming and laborious (Fig. 9C). In addition, this method accounts for total protein quantification in a bulk sample, irrespective of the number of transfected cells. Transfection efficiency can therefore be effectively discriminated with single-cell resolution by flow cytometry. Moreover, transfection efficiency can be discriminated from polymer internalization, thus reinforcing the need for a screening tool enabling the detection of functional RNA delivery [39]. Nevertheless, flow cytometry is often an endpoint assay unless the cells are analyzed and subsequently sorted for further subculturing (in this case cell viability is often

compromised). High-content imaging circumvents this issue and enables longitudinal analysis of fluorescence-based protein expression in live cells.

4. Conclusions

Here, we describe two methods for preparing light-sensitive formulations for RNA therapeutics applications. For this study, we evaluated (i) formulations synthesized with light responsive group in different positions of the polymers structure, (ii) complexation of different RNA molecules, siRNA, miRNA and mRNA, (iii) high-content analysis to identify the best formulations to deliver RNA molecules. This study indicates that the compositional elements of the formulations, other than zeta potential of the NPs, RNA complexation ability, trigger responsiveness, cellular uptake, play a key role in determining an efficient RNA transfection vector. There is tremendous value in optimizing and generating simple libraries of formulations for intracellular delivery of RNA molecules, since transfections often suffer from variable efficacy. Using the appropriate cell model allied with high content analysis we can rapidly monitor several parameters, such as cellular uptake, cytotoxicity, intracellular trafficking and RNA delivery efficacy. Development of technologies/platforms for improving intracellular delivery of RNA-based therapies is of great help to address important research questions in innumerable range of diseases.

Appendices (Materials List)

1. Instrumentation

1.1 Eppendorf Centrifuge 5810R

1.2 IKA KS 4000i control

1.3 Branson 2510 Ultrasonic Cleaner

1.4 Synergy H1 – Microplate Reader

1.5 Brookhaven ZetaPALS BIC

1.6 Sartorius QUINTX35-1S

1.7 Eppendorf Multichannel pipette

1.8 InCell 2200 (GE Healthcare)

2. Reagents and consumables

2.1 Dimethyl sulfoxide (DMSO anhydrous, Sigma-Aldrich, #276855)

2.2 Eppendorf Tubes, 2.0 ml

2.3 96-deepwell plate (polypropylene, VWR, #76329)

2.4 Water, molecular biology grade (Fisher bioreagents, #BP2819)

2.5 96-well plate aluminum cover foil (VWR, #76005)

2.6 Monomers

Monomer	Chemical Name IUPAC	CAS	Vendor
A	Methylenebisacrylamide	110-26-9	Aldrich
B	Hexamethylenebisacrylamide	7150-41-6	Polyscience
C	Cystaminebisacrylamide	6098-457-8	Polyscience
D	Dihydroxyethylenebisacrylamide	868-63-3	Aldrich
E	Bisacryloylpiperazin	6342-17-2	Sigma
P1	(2-Nitro-1,3-phenylene)bis(methylene)diacrylate	1599460-50-0	Synthesized
1	Ethylenediamine	107-15-3	Merck
2	1,4-Diaminobutan	110-60-1	Aldrich
3	1,6-Diaminohexan	124-09-4	Alfa Aesar
4	Diethylenetriamine	111-40-0	Alfa Aesar
5	Triethylenetetraamine	112-24-3	Acros Organics
6	Pentaethylenehexamine	4067-16-7	Aldrich
7	3,3'-Diamino-N-methyldipropylamine	105-83-9	Aldrich
8	1,2-Diaminocyclohexane	694-83-7	Aldrich
9	1,8-Diamino-3,6-dioxaoctane	929-59-9	Acros Organics
10	1,13-Diamino-4,7,10-trioxatridecane	4246-51-9	Aldrich
11	1,4-Bis(aminopropyl)piperazine	7209-38-3	Aldrich
12	1,4-Phenylenedimethanamine	539-48-0	Merck
13	1,5-Diaminonaphthalene	2243-62-1	Aldrich
14	4,4'-methylenedianiline	101-77-9	Aldrich
15	1,3-Phenylenediamine	108-45-2	TCI Chemicals
16	1,3-Diaminopropane	109-76-2	TCI Chemicals
17	2,2-Dimethyl-1,3-propanediamine	7328-91-8	TCI Chemicals
18	1,3-Diaminopentane	589-37-7	TCI Chemicals
19	2,2'-Diamino-N-methyldiethylamine	4097-88-5	TCI Chemicals
20	Agmatine sulfate	2482-00-0	TCI Chemicals
21	1,4-Bis(aminomethyl)cyclohexane	2579-20-6	TCI Chemicals
22	4,4'-Methylenebis(cyclohexylamine)	1761-71-3	Aldrich
23	4,4'-Diaminobenzanilide	785-30-8	Aldrich
24	DL-Lysine	70-53-1	Aldrich
25	3-Amino-1-propanol	156-87-6	Aldrich
26	4-Amino-1-butanol	13325-10-5	Aldrich
27	5-Amino-1-pentanol	2508-29-4	Sigma Aldrich
28	6-Amino-1-hexanol	4048-33-3	Alfa Aesar
29	1-(3-Aminopropyl)pyrrolidine	23159-07-1	Alfa Aesar
30	1-(3-Aminopropyl)imidazole	5036-48-6	Aldrich
31	1-(3-Aminopropyl)-4-methylpiperazine	224-954-4	Alfa Aesar
32	Histamine	51-45-6	Sigma Aldrich

3. Software

3.1 ZetaPlus™ Particle Sizing Software (version 4.03)

3.2 In Cell Developer software (GE Healthcare)

3.3 GraphPad Prism (version 6.0h)

*** Hints for troubleshooting**

- For the preparation of nanoparticles, add the zinc sulfate within 30s after adding the polymer to the water.
- Remember to maximize incident power at start of first measurement in DLS to determine count decrease.
- Remember to always use a freshly prepared batch of RNA@NPs to incubate with cells

*** Highlights**

- A method is defined to efficiently conjugate RNA therapeutics with a light-responsive and biocompatible delivery platform
- A strategy is defined based on high-content imaging analysis to find the best formulation to target specific cell populations with high delivery efficiency
- The synthesis pathway of NPs is inexpensive, simple fabrication and facile purification and storage

Acknowledgements

The authors would like to thank the financial support of ERA Chair project (ERA@UC, ref:669088) through EU Horizon 2020 program, the POCI-01-0145-FEDER-016390 (acronym: CANCEL STEM), POCI-01-0145-FEDER-029414 (acronym: LIghtBRARY) and UID/NEU/04539/2019 projects through Compete 2020 and FCT programs.

*** References**

[1] Y. Dong, D.J. Siegwart, D.G. Anderson, Strategies, design, and chemistry in siRNA delivery systems, Adv Drug Deliv Rev 144 (2019) 133-147.
[2] P.S. Kowalski, A. Rudra, L. Miao, D.G. Anderson, Delivering the Messenger: Advances in Technologies for Therapeutic mRNA Delivery, Mol Ther 27(4) (2019) 710-728.
[3] M.R. Molla, P.A. Levkin, Combinatorial Approach to Nanoarchitectonics for Nonviral Delivery of Nucleic Acids, Adv Mater 28(6) (2016) 1159-75.
[4] H. Shin, S.-J. Park, Y. Yim, J. Kim, C. Choi, C. Won, D.-H. Min, Recent Advances in RNA Therapeutics and RNA Delivery Systems Based on Nanoparticles, Advanced Therapeutics 1(7) (2018) 1800065.

[5] S.F. Dowdy, Overcoming cellular barriers for RNA therapeutics, Nat Biotechnol 35(3) (2017) 222-229.
[6] C.J. Bishop, K.L. Kozielski, J.J. Green, Exploring the role of polymer structure on intracellular nucleic acid delivery via polymeric nanoparticles, J Control Release 219 (2015) 488-499.
[7] D.J. Gary, N. Puri, Y.Y. Won, Polymer-based siRNA delivery: perspectives on the fundamental and phenomenological distinctions from polymer-based DNA delivery, J Control Release 121(1-2) (2007) 64-73.
[8] H. Yin, R.L. Kanasty, A.A. Eltoukhy, A.J. Vegas, J.R. Dorkin, D.G. Anderson, Non-viral vectors for gene-based therapy, Nat Rev Genet 15(8) (2014) 541-55.
[9] Z. Liu, Z. Zhang, C. Zhou, Y. Jiao, Hydrophobic modifications of cationic polymers for gene delivery, Progress in Polymer Science 35(9) (2010) 1144-1162.
[10] L.J. van der Aa, P. Vader, G. Storm, R.M. Schiffelers, J.F. Engbersen, Optimization of poly(amido amine)s as vectors for siRNA delivery, J Control Release 150(2) (2011) 177-86.
[11] M.S. Shim, Y.J. Kwon, Controlled cytoplasmic and nuclear localization of plasmid DNA and siRNA by differentially tailored polyethylenimine, J Control Release 133(3) (2009) 206-13.
[12] F. Ercole, T.P. Davis, R.A. Evans, Photo-responsive systems and biomaterials: photochromic polymers, light-triggered self-assembly, surface modification, fluorescence modulation and beyond, Polym. Chem. 1(1) (2010) 37-54.
[13] Y. Li, Y. He, X. Tong, X. Wang, Photoinduced deformation of amphiphilic azo polymer colloidal spheres, J Am Chem Soc 127(8) (2005) 2402-3.
[14] Y. Zhao, Photocontrollable block copolymer micelles: what can we control?, Journal of Materials Chemistry 19(28) (2009) 4887.
[15] A. Wittrup, A. Ai, X. Liu, P. Hamar, R. Trifonova, K. Charisse, M. Manoharan, T. Kirchhausen, J. Lieberman, Visualizing lipid-formulated siRNA release from endosomes and target gene knockdown, Nat Biotechnol 33(8) (2015) 870-6.
[16] J. Blersch, V. Francisco, C. Rebelo, A. Jimenez-Balsa, H. Antunes, C. Gonzato, S. Pinto, S. Simoes, K. Liedl, K. Haupt, L. Ferreira, A Light-Triggerable Nanoparticle Library for the Controlled Release of Non-Coding RNAs, Angew Chem Int Ed Engl 59(5) (2020) 1985-1991.
[17] J. Blersch, V. Francisco, C. Rebelo, A. Jimenez-Balsa, H. Antunes, S. Pinto, S. Simoes, A. Rai, L. Ferreira, A light-triggerable formulation to control the stability of pro-angiogenic transcription factor hypoxia inducible factor-1alpha (HIF-1alpha), Nanoscale 12(18) (2020) 9935-9942.
[18] H. Bae, H. Chu, F. Edalat, J.M. Cha, S. Sant, A. Kashyap, A.F. Ahari, C.H. Kwon, J.W. Nichol, S. Manoucheri, B. Zamanian, Y. Wang, A. Khademhosseini, Development of functional biomaterials with micro- and nanoscale technologies for tissue engineering and drug delivery applications, J Tissue Eng Regen Med 8(1) (2014) 1-14.
[19] E. Will, H. Klump, N. Heffner, M. Schwieger, B. Schiedlmeier, W. Ostertag, C. Baum, C. Stocking, Unmodified Cre recombinase crosses the membrane, Nucleic Acids Res 30(12) (2002) e59.
[20] B.D. Mather, K. Viswanathan, K.M. Miller, T.E. Long, Michael addition reactions in macromolecular design for emerging technologies, Progress in Polymer Science 31(5) (2006) 487-531.
[21] A. Mangraviti, S.Y. Tzeng, K.L. Kozielski, Y. Wang, Y. Jin, D. Gullotti, M. Pedone, N. Buaron, A. Liu, D.R. Wilson, S.K. Hansen, F.J. Rodriguez, G.D. Gao, F. DiMeco, H. Brem, A.

Olivi, B. Tyler, J.J. Green, Polymeric nanoparticles for nonviral gene therapy extend brain tumor survival in vivo, ACS Nano 9(2) (2015) 1236-49.
[22] D.J. Siegwart, K.A. Whitehead, L. Nuhn, G. Sahay, H. Cheng, S. Jiang, M. Ma, A. Lytton-Jean, A. Vegas, P. Fenton, C.G. Levins, K.T. Love, H. Lee, C. Cortez, S.P. Collins, Y.F. Li, J. Jang, W. Querbes, C. Zurenko, T. Novobrantseva, R. Langer, D.G. Anderson, Combinatorial synthesis of chemically diverse core-shell nanoparticles for intracellular delivery, Proc Natl Acad Sci U S A 108(32) (2011) 12996-3001.
[23] A. Akinc, D.M. Lynn, D.G. Anderson, R. Langer, Parallel synthesis and biophysical characterization of a degradable polymer library for gene delivery, J Am Chem Soc 125(18) (2003) 5316-23.
[24] A. Akinc, D.G. Anderson, D.M. Lynn, R. Langer, Synthesis of poly(beta-amino ester)s optimized for highly effective gene delivery, Bioconjug Chem 14(5) (2003) 979-88.
[25] C. Lin, Z. Zhong, M.C. Lok, X. Jiang, W.E. Hennink, J. Feijen, J.F.J. Engbersen, Linear poly(amido amine)s with secondary and tertiary amino groups and variable amounts of disulfide linkages: Synthesis and in vitro gene transfer properties, Journal of Controlled Release 116(2) (2006) 130-137.
[26] X. Deng, N. Zheng, Z. Song, L. Yin, J. Cheng, Trigger-responsive, fast-degradable poly(beta-amino ester)s for enhanced DNA unpackaging and reduced toxicity, Biomaterials 35(18) (2014) 5006-15.
[27] K. Zeilinger, N. Freyer, G. Damm, D. Seehofer, F. Knospel, Cell sources for in vitro human liver cell culture models, Exp Biol Med (Maywood) 241(15) (2016) 1684-98.
[28] M. Obinata, The immortalized cell lines with differentiation potentials: their establishment and possible application, Cancer Sci 98(3) (2007) 275-83.
[29] S. Domcke, R. Sinha, D.A. Levine, C. Sander, N. Schultz, Evaluating cell lines as tumour models by comparison of genomic profiles, Nat Commun 4 (2013) 2126.
[30] C.D. Sago, M.P. Lokugamage, K. Paunovska, D.A. Vanover, C.M. Monaco, N.N. Shah, M. Gamboa Castro, S.E. Anderson, T.G. Rudoltz, G.N. Lando, P. Munnilal Tiwari, J.L. Kirschman, N. Willett, Y.C. Jang, P.J. Santangelo, A.V. Bryksin, J.E. Dahlman, High-throughput in vivo screen of functional mRNA delivery identifies nanoparticles for endothelial cell gene editing, Proc Natl Acad Sci U S A 115(42) (2018) E9944-E9952.
[31] N. Sultana, A. Magadum, Y. Hadas, J. Kondrat, N. Singh, E. Youssef, D. Calderon, E. Chepurko, N. Dubois, R.J. Hajjar, L. Zangi, Optimizing Cardiac Delivery of Modified mRNA, Mol Ther 25(6) (2017) 1306-1315.
[32] J.C. Kaczmarek, K.J. Kauffman, O.S. Fenton, K. Sadtler, A.K. Patel, M.W. Heartlein, F. DeRosa, D.G. Anderson, Optimization of a Degradable Polymer-Lipid Nanoparticle for Potent Systemic Delivery of mRNA to the Lung Endothelium and Immune Cells, Nano Lett 18(10) (2018) 6449-6454.
[33] A. Nagy, Cre recombinase: the universal reagent for genome tailoring, Genesis 26(2) (2000) 99-109.
[34] L. Ciani, S. Ristori, C. Bonechi, C. Rossi, G. Martini, Effect of the preparation procedure on the structural properties of oligonucleotide/cationic liposome complexes (lipoplexes) studied by electron spin resonance and Zeta potential, Biophys Chem 131(1-3) (2007) 80-7.
[35] P. Vader, L.J. van der Aa, J.F. Engbersen, G. Storm, R.M. Schiffelers, Disulfide-based poly(amido amine)s for siRNA delivery: effects of structure on siRNA complexation, cellular uptake, gene silencing and toxicity, Pharm Res 28(5) (2011) 1013-22.

[36] S. Jeon, J. Clavadetscher, D.K. Lee, S.V. Chankeshwara, M. Bradley, W.S. Cho, Surface Charge-Dependent Cellular Uptake of Polystyrene Nanoparticles, Nanomaterials (Basel) 8(12) (2018).
[37] W. Song, L. Popp, J. Yang, A. Kumar, V.S. Gangoli, L. Segatori, The autophagic response to polystyrene nanoparticles is mediated by transcription factor EB and depends on surface charge, J Nanobiotechnology 13 (2015) 87.
[38] R.L. Juliano, X. Ming, K. Carver, B. Laing, Cellular uptake and intracellular trafficking of oligonucleotides: implications for oligonucleotide pharmacology, Nucleic Acid Ther 24(2) (2014) 101-13.
[39] J. Kim, J.C. Sunshine, J.J. Green, Differential polymer structure tunes mechanism of cellular uptake and transfection routes of poly(beta-amino ester) polyplexes in human breast cancer cells, Bioconjug Chem 25(1) (2014) 43-51.

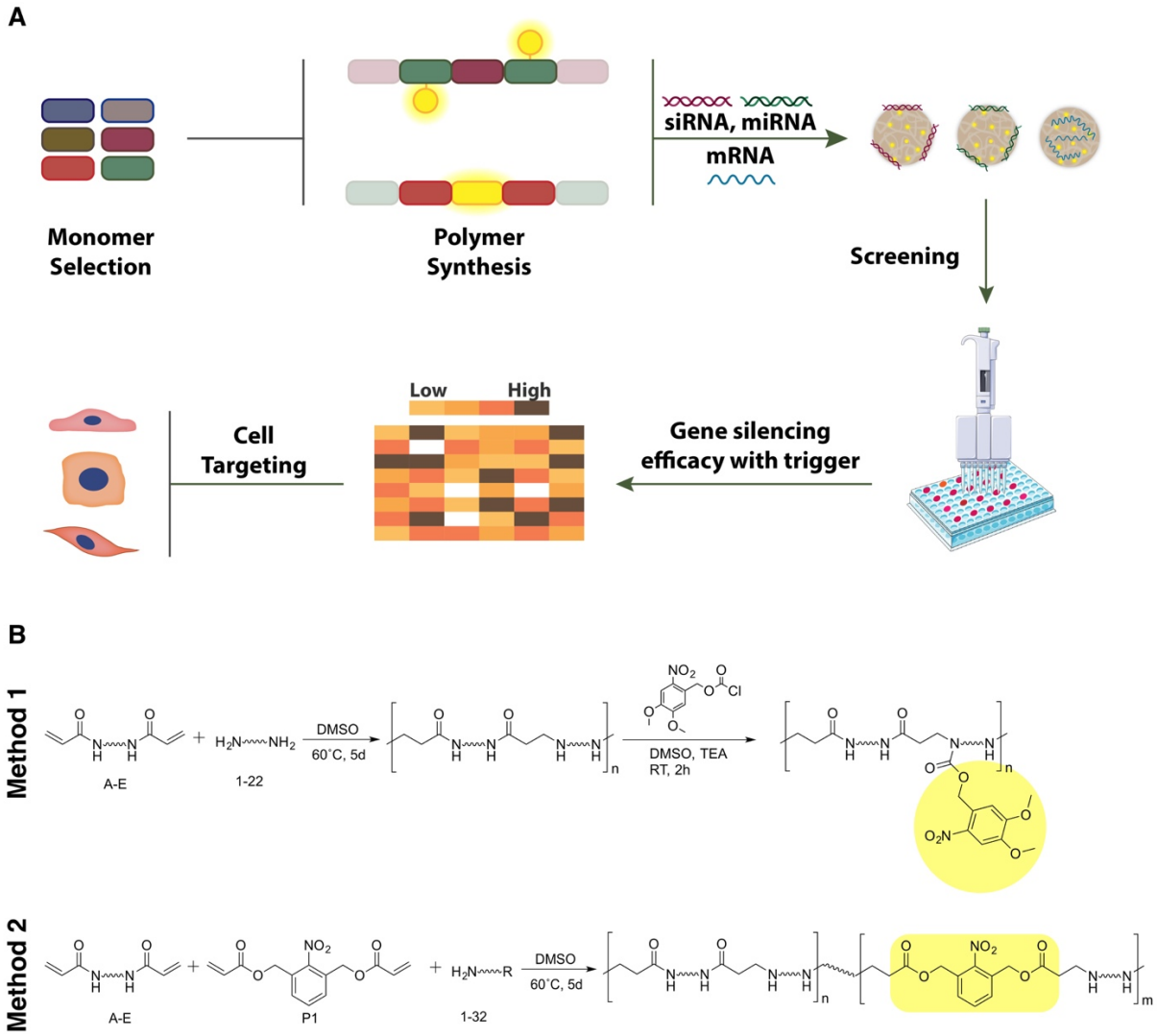

Figure 1. (A) Schematic representation of the steps for high-throughput screening of NP formulations containing RNA-based therapeutics. These steps include: (i) monomer selection, (ii) polymer synthesis, (iii) RNA molecules complexation, (iv) efficacy assay and (v) cell targeting assay. (B) Reaction scheme for the synthesis of poly(amido amine)s polymers with light sensitive moieties attached in the side-chain as a pendant (method 1) or incorporated onto polymers chain backbone (method 2).

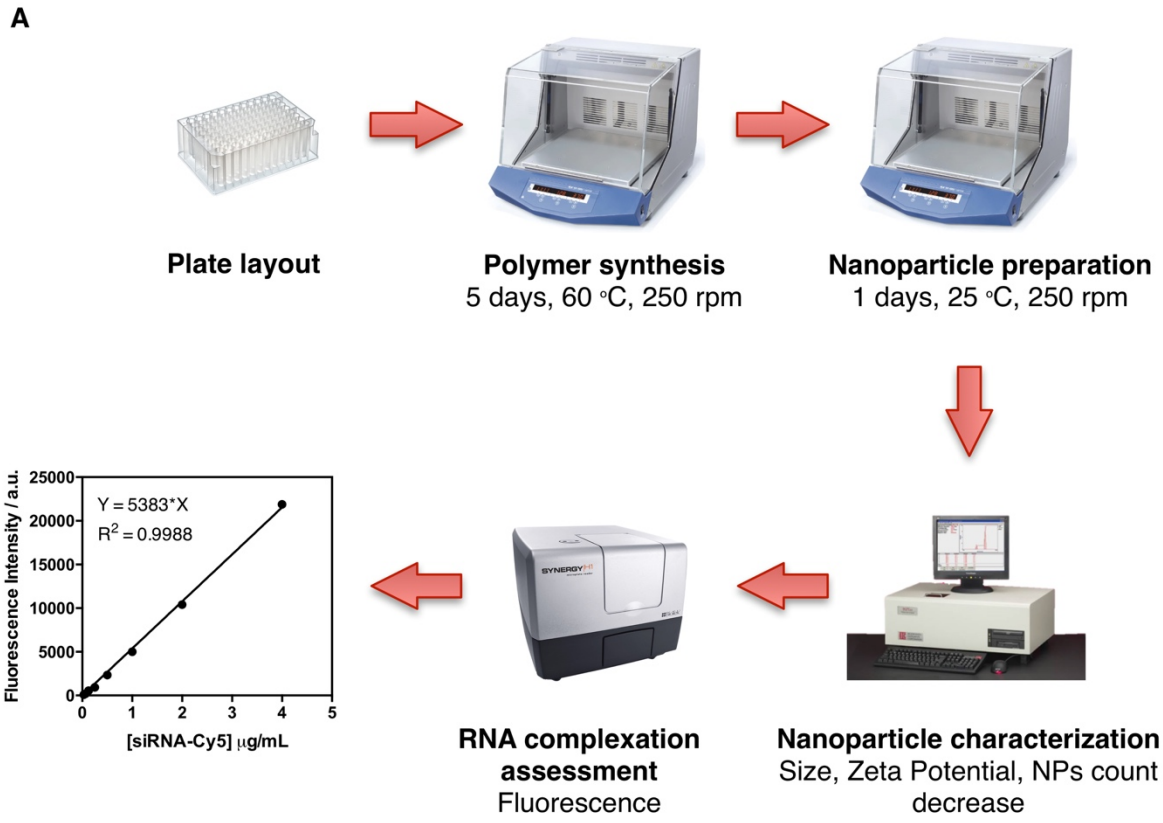

Figure 2. Scheme for nanoparticle formation, complexation and quantification of RNA molecules.

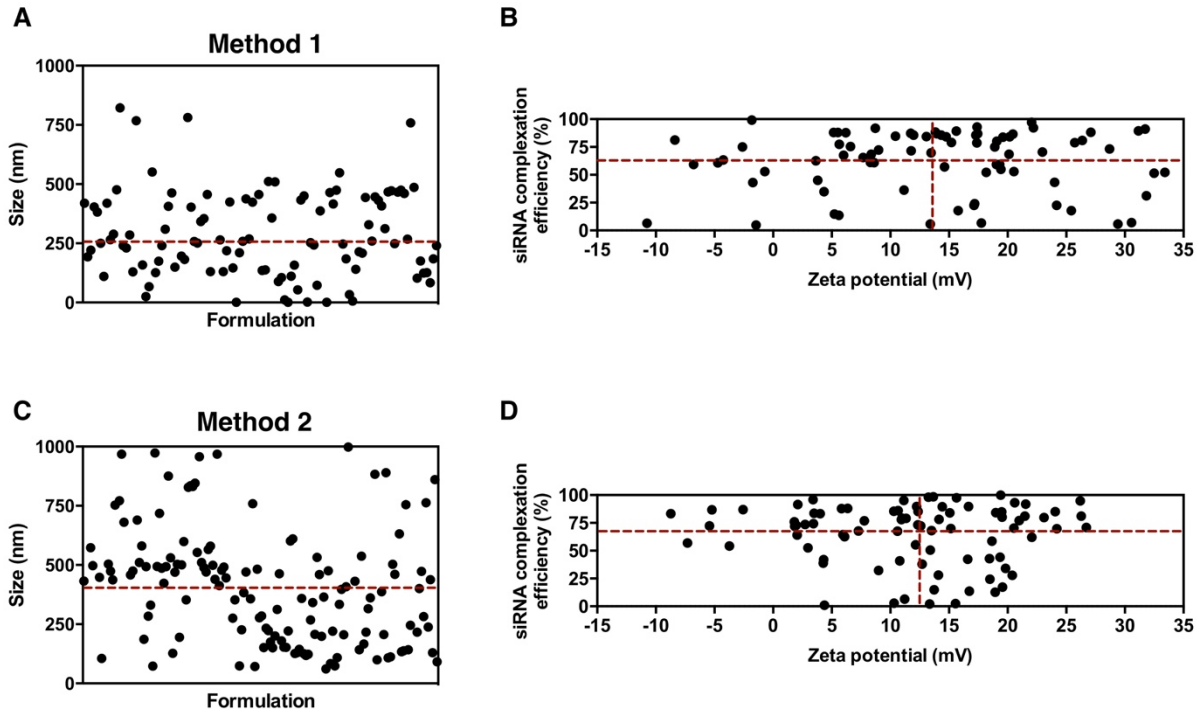

Figure 3. Physicochemical properties of NPs assembled after nanoprecipitation of polymers synthesised through method 1 and 2. (A) Size of NPs formed using method 1 determined by DLS (50 µg/mL). Dashed red line indicate average NPs size. (B) Correlation between NPs zeta potential and siRNA complexation efficiency in method 1. Complexation efficacy was determined indirectly from Cy5 tagged-siRNA after separating NPs and non-complexed siRNA by centrifugation. Concentration of siRNA was determined relative to a standard curve. Dashed red line indicate average NPs zeta potential and siRNA complexation efficiency. (C) Size of NPs formed using method 2 determined by DLS (50 µg/mL). (D) Correlation between NPs zeta potential and siRNA complexation efficiency in method 2.

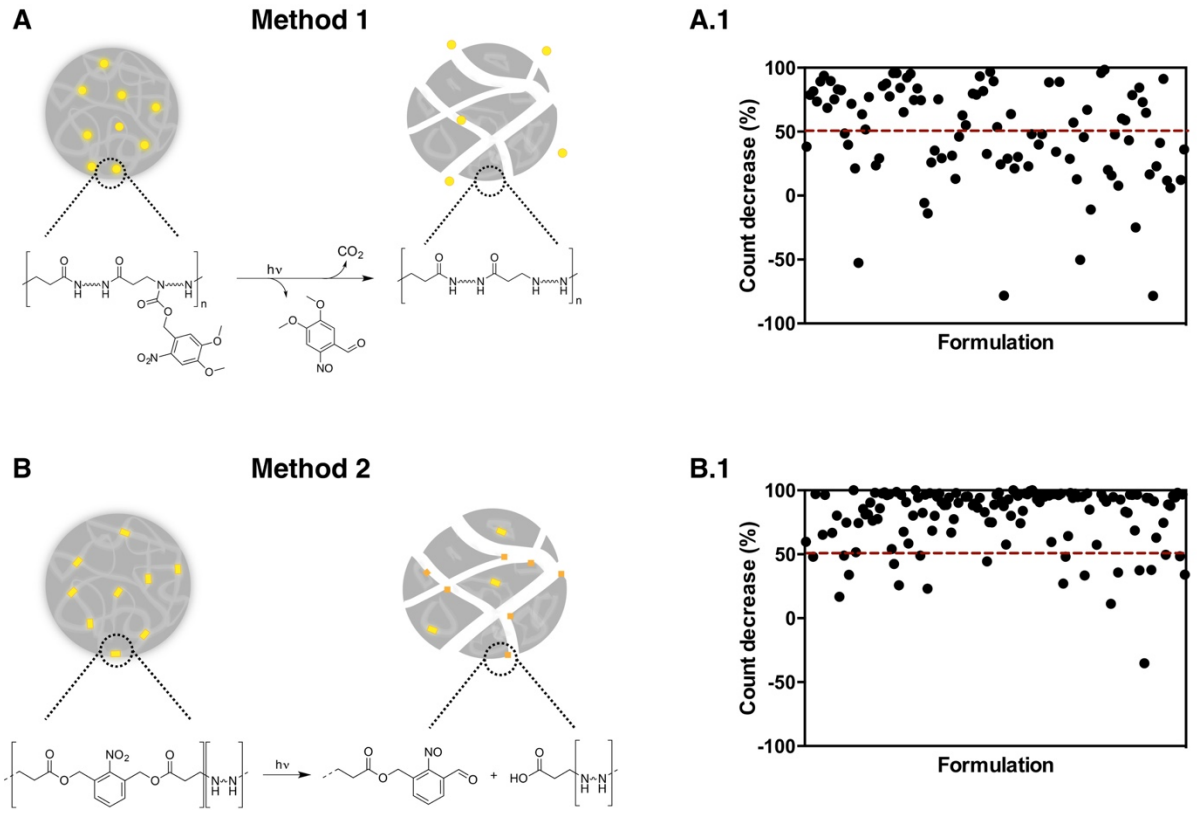

Figure 4. Schematic representation of the nanoparticle disassembly upon UV light irradiation. (A) The cleavage of NVOC moiety in polymers synthesised through method 1 leads to NPs disassembly due to change in the hydrophilic/hydrophobic balance. (A.1) NPs count decrease upon UV light irradiation of formulation, determined by DLS after 10 min UV irradiation ([NPs] = 50 μg/mL, λ = 365 nm, 100 mW/cm^2). NP count decrease is expressed as percent count decrease respective to the initial NP average count rate. 52.5% of formulations had a NPs count decrease higher than 50 % (dashed red line). (B) The generation of the nitrobenzene group due to cleavage of the photo-responsive ester bond leads to NPs disassembly in formulation formed with polymers synthesised through method 2. (B.1) NPs count decrease upon UV light irradiation of formulation, determined by DLS after 10 min UV irradiation ([NPs] = 50 μg/mL, λ = 365 nm, 100 mW/cm^2). 82.7% of formulations had a NPs count decrease higher than 50 % (dashed red line).

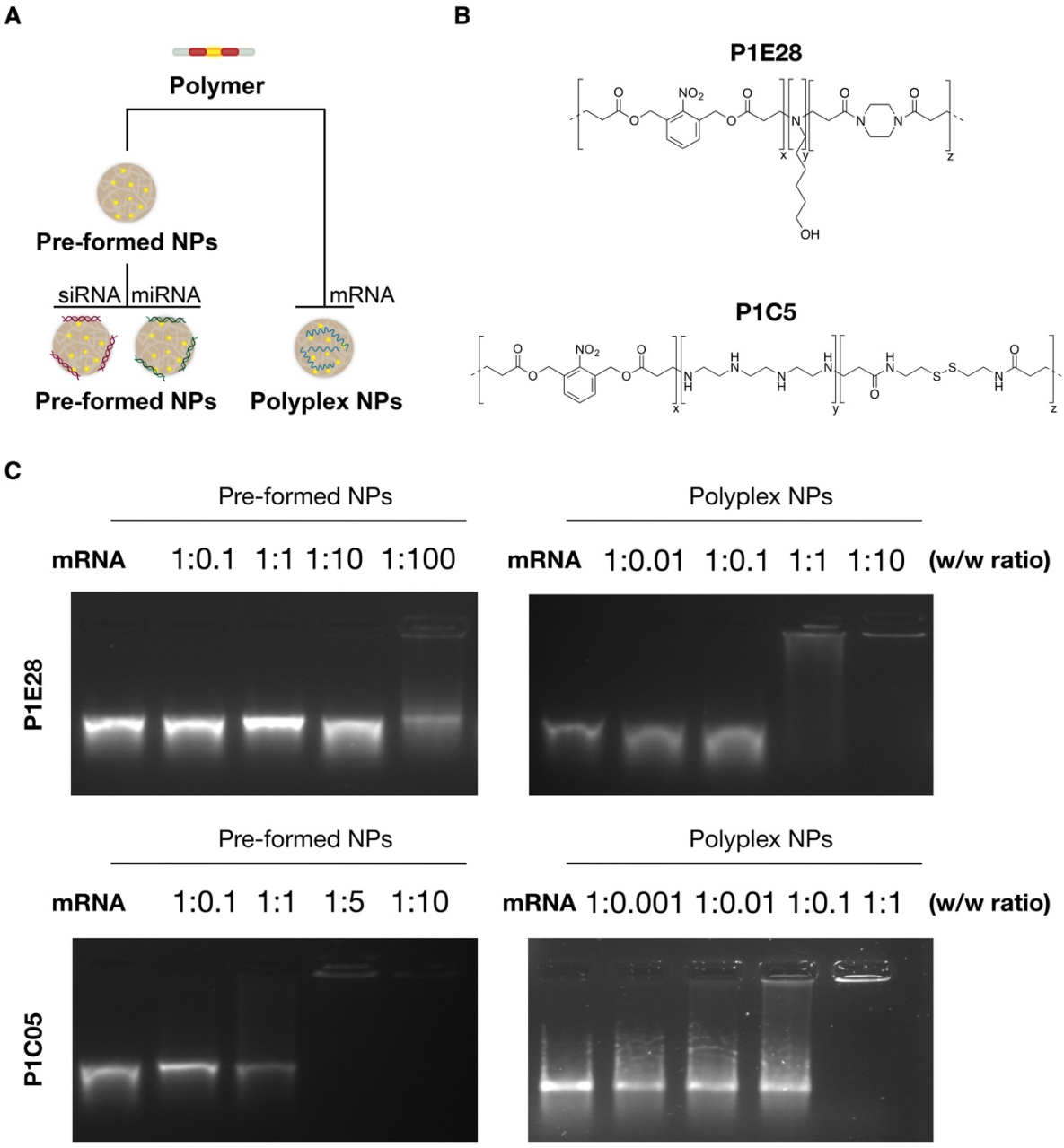

Figure 5. (A) Schematic representation of different pathways to complex RNA therapeutics, siRNA, miRNA and mRNA with polymers. (B) Chemical structure of P1E28 and P1C5 polymers. (C) Gel retardation profiles of pre-formed NPs and polyplex NPs from P1E28 and P1C5 polymers at w/w ratios (mRNA/polymer) from 0.1 to 100.

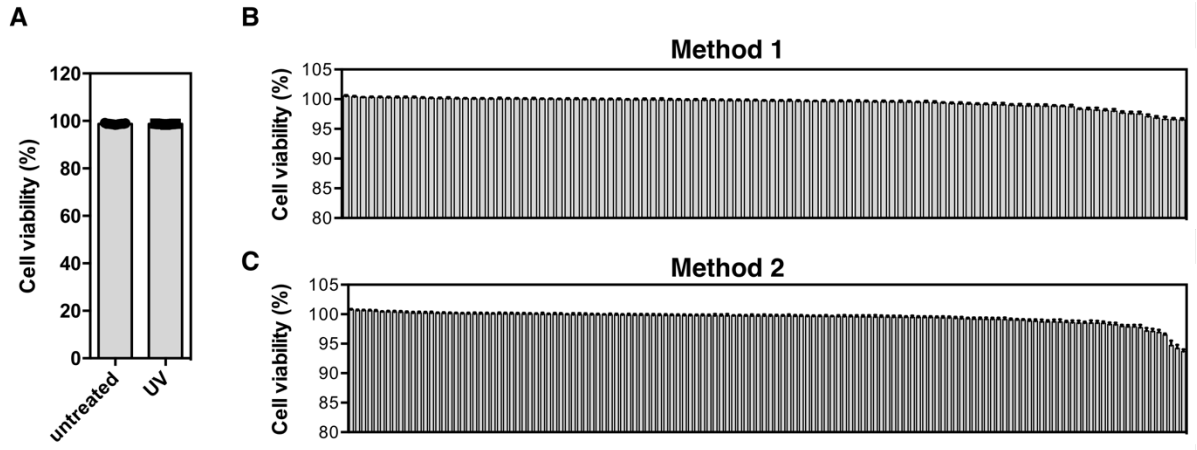

Figure 6. Influence of UV light on cell viability. (A) Cell viability of HeLa-GFP cells. Cells were irradiated or not with UV light (10 min, 1 mW/cm^2) and analyzed at 48 h post transfection. Cell nuclei were stained with Hoechst H33342 and propidium iodide at 48 h, and cell viability calculated as the % of dead nuclei from the total count of nuclei. Results are presented as Mean ± SEM (n = 6). (B) and (C) Cell viability at 48 h post transfection with NPs@siRNA (20 µg/mL, method 1 and 2) for 4 h and irradiated with UV light. Results are presented as Mean ± SEM (n = 3).

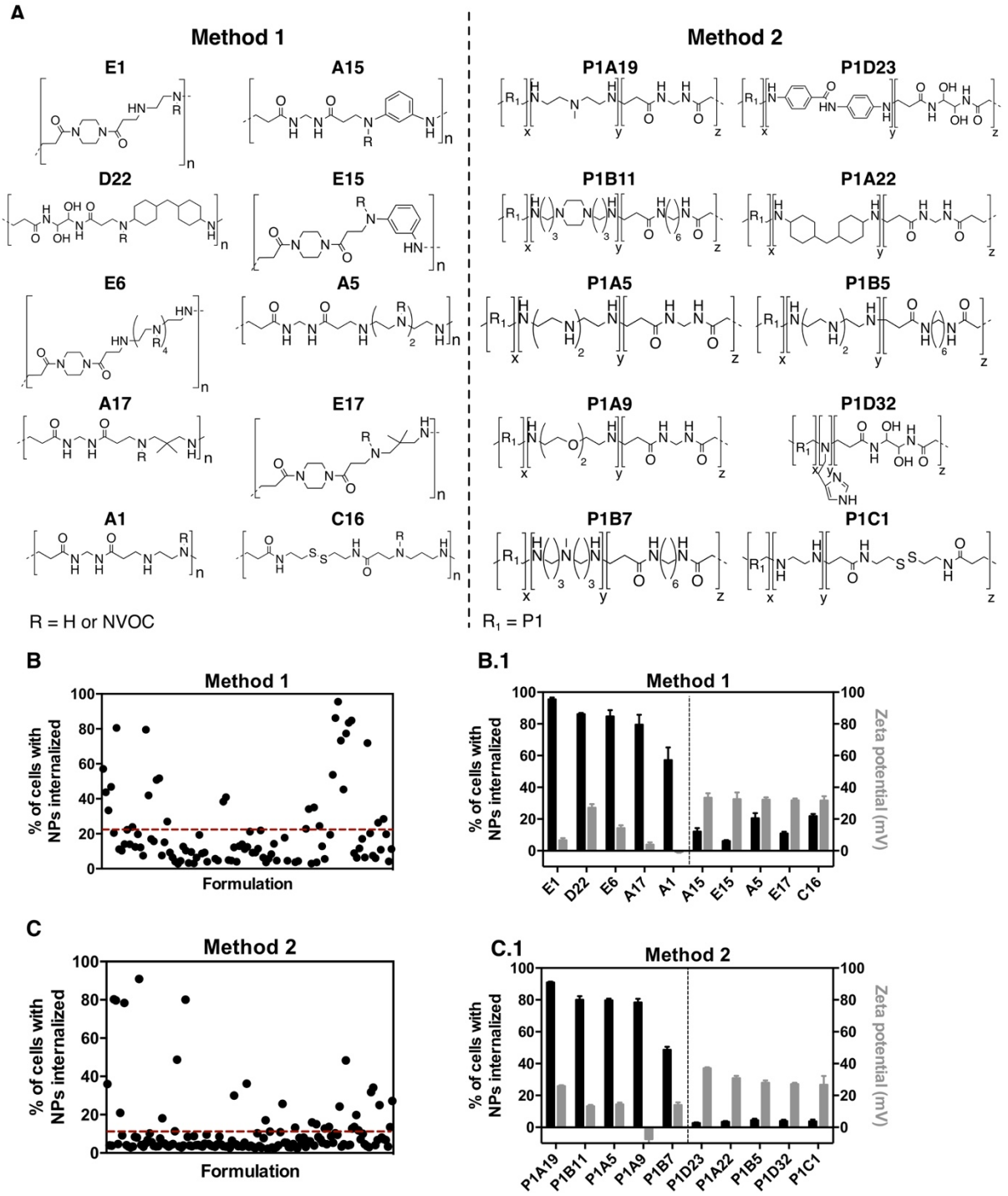

Figure 7. Cellular uptake of NP@siRNA-Cy5 formulations. (A) Chemical structure of the best formulations with highest cellular uptake or zeta potential. Percentage of HeLa cells stained with NP@siRNA-Cy5 by method 1 (B) and method 2 (C) transfected for 10 min (20 µg/mL), washed and UV irradiated (10 min, 365 nm, 1 mW/cm^2). Correlation between the best 5 formulations with highest percentage of cells with NPs internalised or highest zeta potential by method 1 (B.1) and method 2 (C.1). The zeta potential of NPs (50 µg/mL) was determined in a KCl solution (1 mM) by DLS. Results are presented as Mean ± SEM (n = 3).

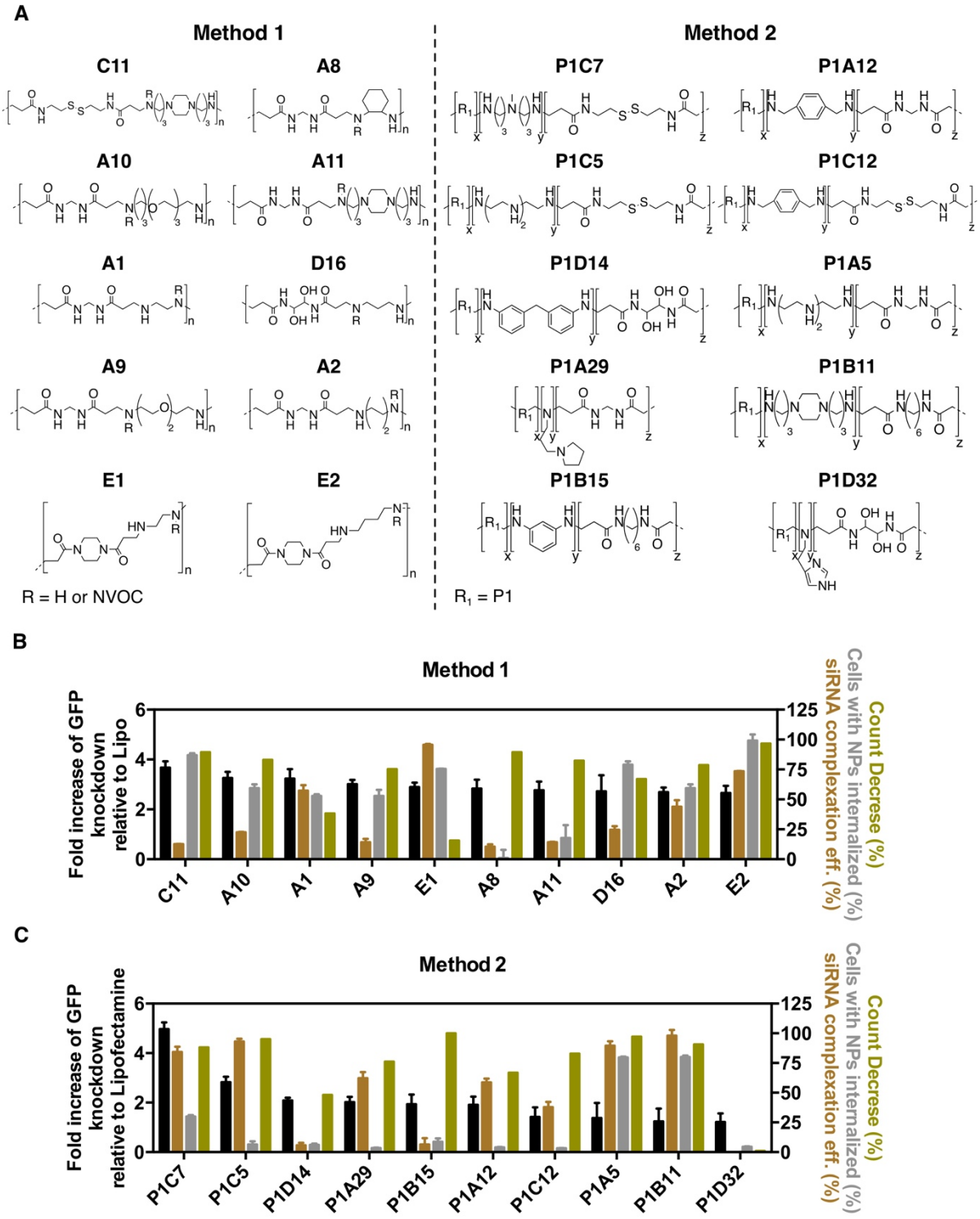

Figure 8. Chemical structures and correlation between gene knockdown activity with physicochemical properties of NPs assembled by method 1 (A and B) and method 2 (A and C) of the top 10 formulations. Fold increase of HeLa GFP knockdown after 48 h post transfection (transfection time for 10 min, 20 μg/mL, washed and irradiated with UV light for 10 min, 365 nm, 1 mW/cm^2) relative to Lipofectamine. Results are presented as Mean ± SEM (n = 3).

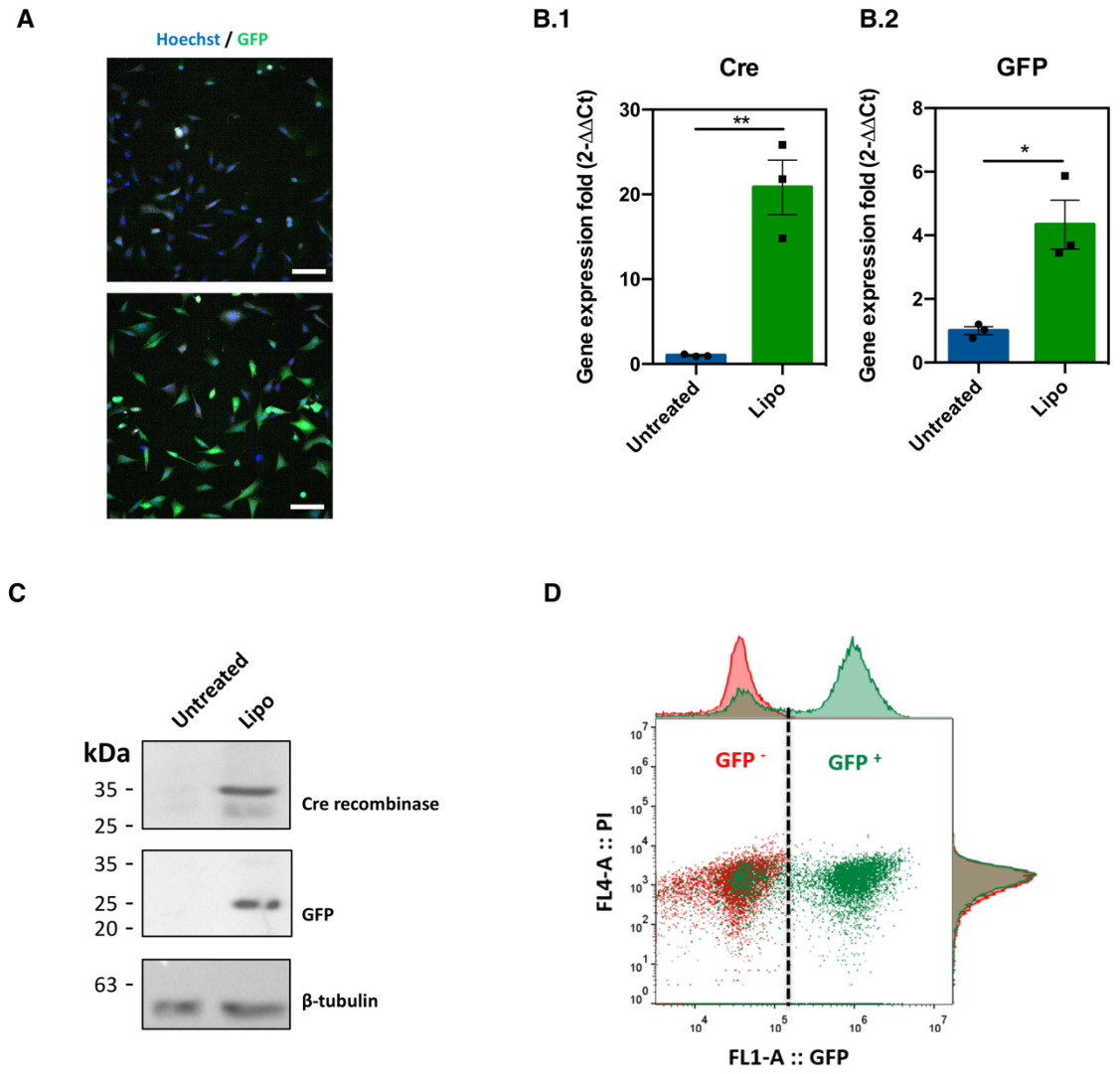

Figure 9. Comparison of different methods used to evaluate transfection efficiency of RNA delivery vectors. Lipofectamine 2000-mediated transfection of Cre reporter fibroblasts with mRNA encoding Cre recombinase was used as an example. Cre reporter fibroblasts were transfected for 4h and the expression of Cre recombinase resulted in cell recombination and expression of a GFP fluorescent reporter protein. (A) High-content imaging performed 48h post-trasnfection enabled the identification and quantification of transfected cells with single-cell resolution. Scale bar=100µm. (B) qRT-PCR was used to quantify the relative abundance of Cre and GFP mRNA to infer protein expression. Gene expression was normalized by the housekeeping gene GAPDH. Results are mean ± SEM (n = 3). Statistical analysis was assessed by unpaired student t-test. * P<0.05, **P<0.01. (C) Protein extracts (20µg/lane) analyzed by Western blot confirm the presence of both proteins in conditions transfected with the mRNA. This quantitative technique can specifically determine the amount of protein expression, albeit lacking single cell resolution. (D) Flow cytometry quantified protein expression at a single-cell level. The dotplot shows a clear GFP+ cell population that is only

present after Cre mRNA transfection (in green) and that differs in GFP signal/expression with untreated conditions (in red).